THE JOURNAL OF PHYSICAL CHEMISTRY B
A JOURNAL OF THE AMERICAN CHEMICAL SOCIETY

pubs.acs.org/JPCB

Article

Glyco-Ligated Binders to Lectins: Multivalency vs Specificity

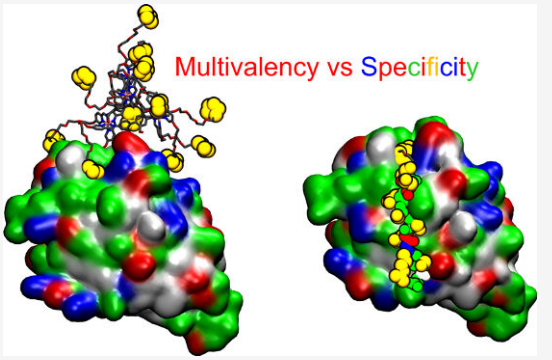
Roya Jafari and Petr Král*

Cite This: https://doi.org/10.1021/acs.jpcb.6c01091

Read Online

ACCESS | Metrics & More | Article Recommendations

ABSTRACT: Here, we examine and compare different types of glycan-based binders to lectins, a class of carbohydrate-binding proteins involved in many biological recognition processes. We use atomistic molecular dynamics simulations to model metallosupramolecular glycoassemblies of different topologies, core charges, and linker lengths binding in a multivalent manner to glyco-recognizing domains in Concanavalin A (ConA), a well-studied plant lectin with specific affinity for mannose and glucose. We also designed and modeled a small peptidoglycan specifically bound to ConA. The obtained results reveal that despite their small size, simple peptidoglycans can have strong affinities to lectins, comparable to large multivalent supramolecular binders.



Downloaded via Petr Kral on July 10, 2026 at 14:40:11 (UTC).
See https://pubs.acs.org/sharingguidelines for options on how to legitimately share published articles.

I. INTRODUCTION

Lectins, a class of carbohydrate-binding proteins, mediate a wide range of biological processes in humans, such as intercellular communications, immune responses, and pathogen recognition.[1−3] The biological activities of lectins arise from their ability to recognize and bind specific glycans in their carbohydrate recognition domains (CRDs).[4] This glycan binding can trigger or modulate immune signaling, cellular adhesion, endocytosis, and inflammatory responses.[5,6] Disruption of lectin−glycan interactions has been implicated in numerous pathological conditions, including chronic inflammation, cancer progression, and infectious diseases.[7,8] Consequently, CRDs are attractive targets for therapeutic modulation by lectin binders.[9−13]

In order to target lectin-CRDs, glycan-functionalized polymers,[14,15] peptides,[16,17] dendrimers,[18,19] nanoparticles,[20,21] and other structures have been developed. Multiple glycans attached to these scaffolds can provide multivalent binding to individual or grouped lectins in biological systems.[22−24] The multivalent binding of these glycan-holding constructs is affected by their many structural and chemical parameters.[25] The preparation of such constructs with suitable characteristics remains a significant challenge.[26,27]

Supramolecular metal−organic cages have shown promise across a wide range of biomedical applications, such as drug and gene delivery, or medical imaging.[28−31] Similar metallic complexes with suitable attached ligands can also provide multivalent binding to various receptors.[32−34] When glyco-functionalized, these constructs can act as powerful binders to lectins.[35,36] Recently, metallosupramolecular assemblies of different topologies, core charges, and methyl α-D-mannopyranos-functionaled ligands of different lengths (MSGAs) were shown to bind to Concanavalin A (ConA), a plant lectin derived from jack bean seeds.[37−39] However, these chemically hybrid constructs are relatively large and complex for the required activity.

Here, we use atomistic molecular dynamics (MD) simulations to compare multivalent ConA binding of MSGAs with many nonspecific linkers and a highly specific ConA binding of a much smaller peptidoglycan (PG). These studies could reveal when it might be suitable to replace large multivalent binders of limited specificity with small specific binders based on a more homogeneous chemistry.

II. SIMULATED SYSTEMS

First, we simulate multivalent binding of different MSGAs to ConA. In order to keep ConA in a dimeric form and avoid the formation of cross-linked aggregates, MSGAs-ConA coupling was experimentally studied at low protein concentrations of 82 μM, salt concentrations of c = 0.01 M NaCl, and acidic pH = 4.8.[39] Here, we simulate MSGAs-ConA binding at both the experimental and physiological ionic strengths to figure out the effect of shielding on this binding. To account for the overall nature of MSGAs-ConA coupling, these simulations are done at two coupling settings: when either one of the MSGA-glycans is docked in ConA, or when neither of its glycans is docked. Next, we design a suitable PG and simulate its specific binding to ConA when its glycan is bound in the docking site.

Received: February 17, 2026
Revised: June 19, 2026
Accepted: June 25, 2026

ACS Publications
© XXXX The Authors. Published by American Chemical Society

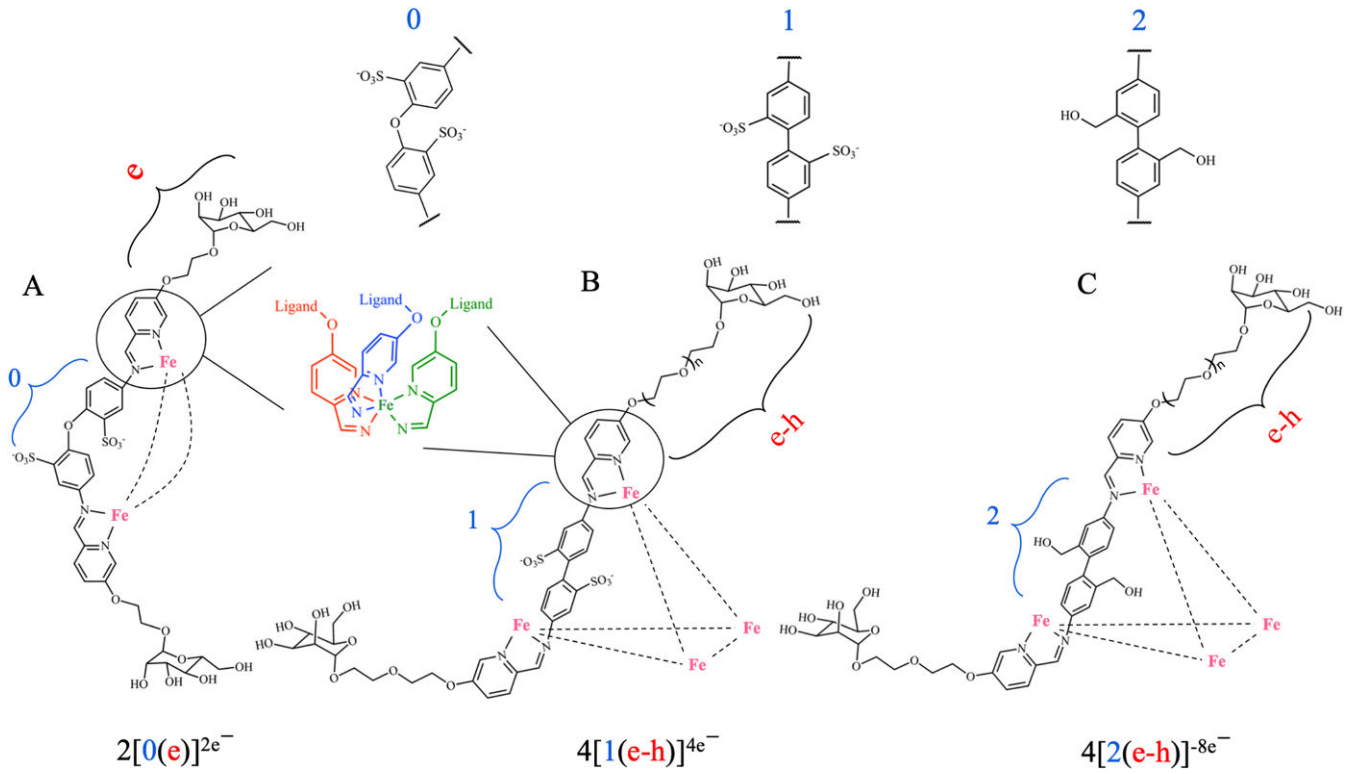


Figure 1. Chemical structures of (A) bimetallic binders (two Fe^{2+} ions, total charge of $2e^-$) and (B, C) tetrametallic tetrahedral binders (four Fe^{2+} ions, total charges of $4e^-$ and $-8e^-$). (top) The (0−2) metal linkers used in (A−C) MSGAs, respectively, are connected to 3 ligands, which are coordinated to Fe^{2+} as depicted. The visualized MSGA structures can be denoted by the formula (A) $2[0(e)]^{2-}$, (B) $4[1(e\text{-}h)]^{4-}$, and (C) $4[2(e\text{-}h)]^{-8e^-}$ (see text).

II.I. Metallosupramolecular Glycan Binders of ConA

Figure 1 shows schematics of simulated MSGAs based on multi-Fe^{2+} cages with ligands attached at each metal. The MSGAs have different topologies, charges, and ethylene glycol (EG) linker lengths. They are denoted as $m[I(n)]^q$, where m is the number of Fe^{2+} ions, I is the (0−2) metal linker, n is the number of the EG monomer ([e]: $n = 0$, [f]: $n = 1$, [g]: $n = 2$, and [h]: $n = 3$), and q is the total charge of MSGA. The ConA monomer was derived from a natural tetramer pdb structure (Section III). The MSGAs-ConA coupling is simulated at (1) the experimental conditions (EC)[39] of $c = 0.01$ M NaCl and pH = 4.8, and (2) the physiological conditions (PC) of $c = 0.15$ M NaCl and $pH = 7.4$. At EC and PC, the total charge of ConA monomer is 0 and $7e^-$, respectively (Section III). In both conditions, two metal cations, Mn^{2+} and Ca^{2+}, are present in ConA within ≈1 nm distance from the glycan binding site and affect the binding of charged MSGAs.

We can perform a qualitative estimation of MSGAs Coulombic coupling to these two ConA metals. In ionic solutions, the Coulombic coupling energy between the charged MSGAs and the two metal ions in ConA can be estimated from

$$E(r_{12}) = \frac{q_1 q_2}{4\pi\varepsilon_r\varepsilon_0 r_{12}} e^{-r_{12}/\lambda_D}, \quad \lambda_D = \sqrt{\frac{\varepsilon_0\varepsilon_r k_B T}{\sum_i \rho_i z_i^2 e^2}} \qquad (1)$$

Here, $q_{1,2}$ are the total charges of MSGAs and ConA metal ions, r_{12} is the average distance of these charges, ε_0 and ε_r are the permittivity of free space and water, respectively, k is the Boltzmann constant, T is the temperature, ρ_i and z_i are the number density and the valency of species i, respectively, and e^- is the elementary charge of an electron. Debye lengths of $\lambda_D \approx$ 3.04 nm (EC) and ≈7.8 Å (PC) are used in eq 1.

Figure 2 shows the Coulombic coupling energies calculated between the centers of mass (CMS) of differently charged

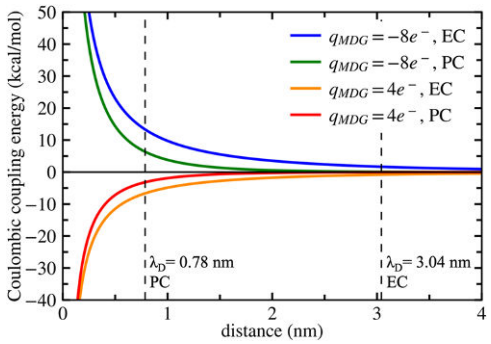


Figure 2. Coulombic coupling energies between differently charged MSGAs (CMS) and two metal ions, Mn^{2+} and Ca^{2+}, that are close to the glycan binding site in ConA. The energies are calculated at EC and PC using a screened Coulombic coupling (eq 1) at different distances between the CMS of each MSGA and the two metals (see text).

MSGAs and the two ConA metal ions. At a typical separation of 2.5 nm (docked glycan, Figure 4A,B) between CMS of MSGA with $q_{MSGA} = 4e^-$ ($-8e^-$) and the ConA metal ions with $q_{metals} = -4e^-$, the Coulombic coupling energy drops by an order of magnitude, from −1.2 to −0.11 kcal/mol (2.4−0.23 kcal/mol), when EC are changed to PC. Therefore, MSGAs are reasonably coupled to both metal ions in EC, but this coupling is largely screened in PC. This means that at physiological conditions, the overall MSGA charges are much less relevant for the ConA binding. During the simulations, the coupling is correctly

https://doi.org/10.1021/acs.jpcb.6c01091
J. Phys. Chem. B XXXX, XXX, XXX−XXX

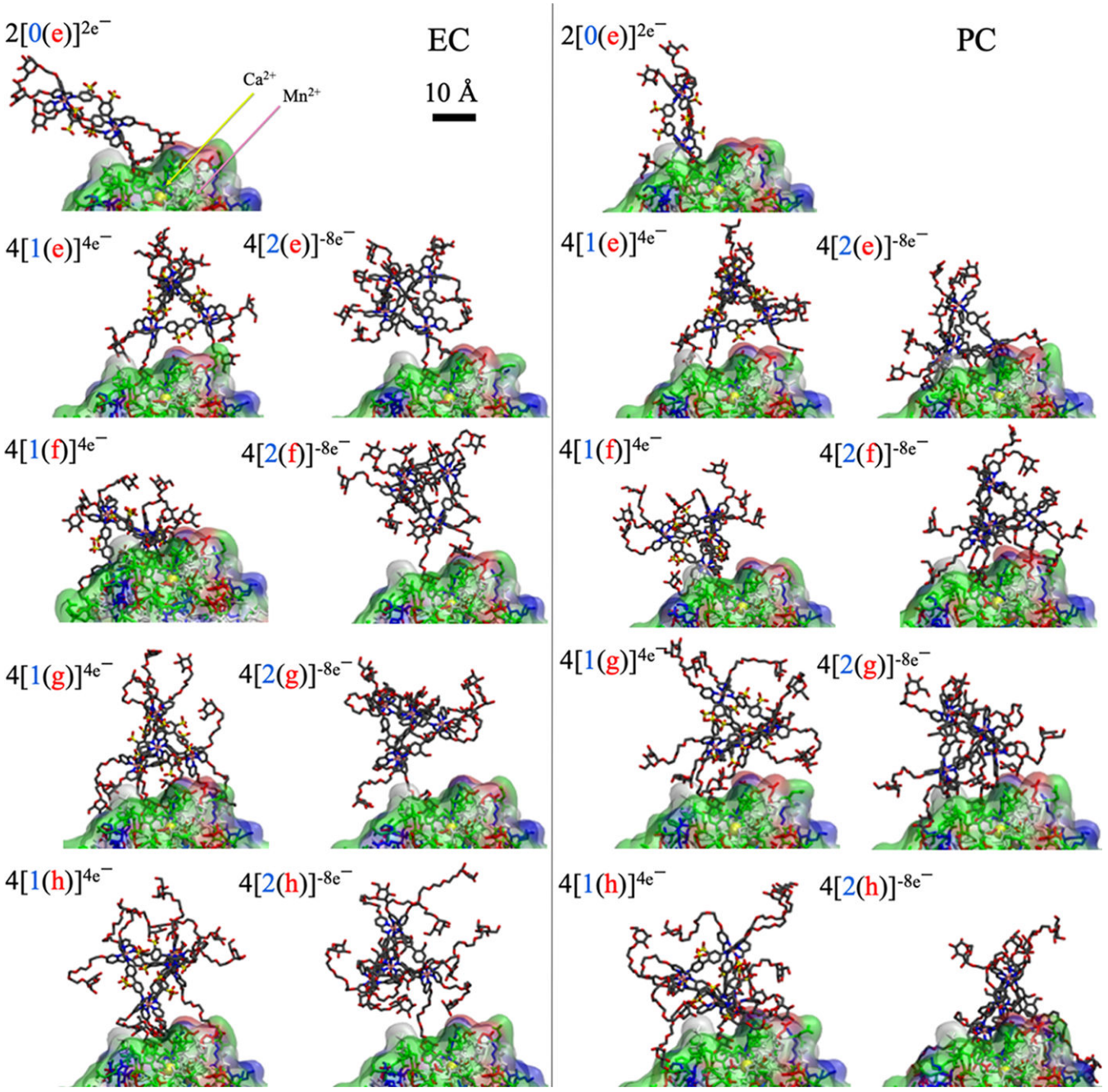


Figure 3. Snapshots of MSGAs glycan-docked to ConA monomer after 200 ns of equilibration (see text). The left two columns display snapshots at EC, with the first column showing negative MSGAs and the second column showing positive ones. The right two columns depict the same at PC.

accounted for by the Particle Mesh Ewald (PME) method (Section III).

II.I.I. Distance Distribution Analysis—Docked MSGAs. Next, we simulate the MSGAs-ConA coupling at EC and PC when one MSGA-glycan was docked in the ConA CRD. Figure 3 shows typical snapshots of the systems simulated for 200 ns. The first and second columns show negatively and positively charged MSGAs coupled to ConA at the EC, respectively. The third and fourth columns show the same at the PC. At EC, Coulombic coupling has a moderate effect on the MSGA-ConA distances. Negatively charged cages are attracted to the two metal cations in ConA, whereas positively charged cages are repelled. This is reflected in the different distances between MSGAs and ConA, depending on the cage charge. However, at PC, the positive and negative MSGAs are at very similar distances from ConA depending on the ligand lengths.

To better understand the MSGA binding of ConA observed in these simulations, shown in Figure 3, we calculate the spatial distributions of MSGAs and their ligands. In Figure 4, we show (left-EC, right-PC) the distributions of MSGA-CMSs (first row) and their glycans (second and third rows) as a function of their distance d from the glycan-docking site. The distributions were averaged over 200 ns trajectories or the actual docking time of the glycan if it undocked sooner.

In Figure 4A,B, we can see that in both solutions, the CMS distances appear arranged according to the MSGA-ligand lengths ([e]−[h]). Moreover, in EC (poor screening), there is a clear difference between oppositely charged MSGAs, where

https://doi.org/10.1021/acs.jpcb.6c01091
J. Phys. Chem. B XXXX, XXX, XXX−XXX

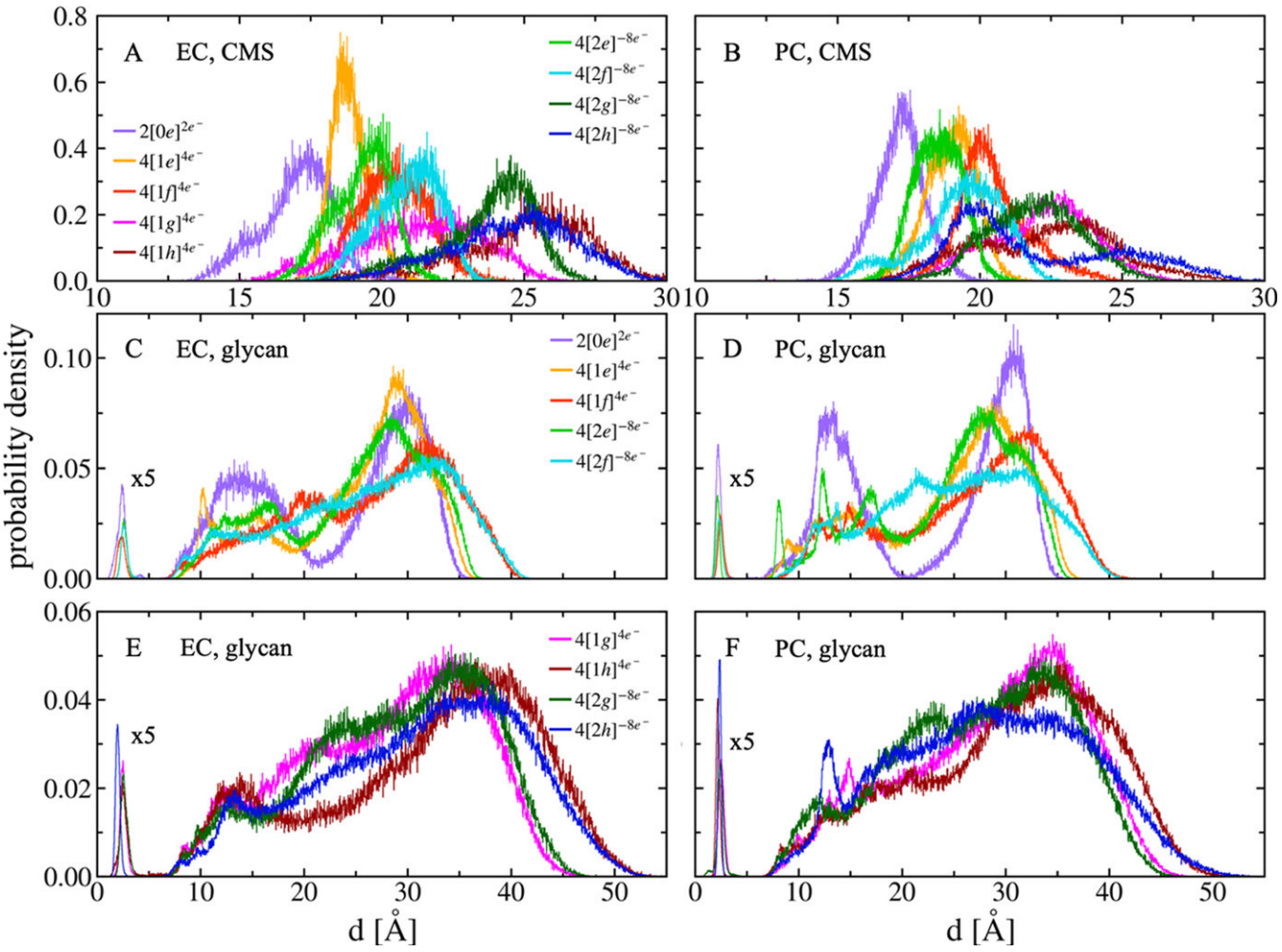


Figure 4. Distributions of MSGA-CMSs (A, B) and MSGA-glycans (C−F) as a function of their distance d from the glycan-docking site, calculated at EC (left) and PC (right). The docked glycan peaks (0−5 Å) need to be multiplied by 5.

the negative MSGAs are closer to the docking site (attracted) and the positive ones are further away (repelled). However, in PC (good screening), oppositely charged MSGAs with the same lengths of ligands have very similar distributions. In some MSGAs with longer ligands, the CMS distributions have several peaks that can be associated with a temporary partial docking of additional glycans.

In Figure 4C−F, we show glycan distributions for MSGAs. The distributions of the docked glycan centered around $d \approx 2.5$ Å are nearly identical. However, the distributions of the undocked glycans ($d \approx 5-55$ Å) are different, but they appear similar in both solutions. MSGAs with shorter ligands have typical two-peak glycan distributions. The first smaller peak ($d \approx 14$ Å) originates from ligands positioned at the same MSGA-metal as the docked glycan, while the second larger peak ($d \approx 30$ Å) originates from the remaining ligands (other metal centers). In MSGAs with longer ligands, which can reach further, the glycan distributions appear more smeared and linearly increasing in size toward the position of the second peak caused by many glycans (shifted to $d \approx 35$ Å). Moreover, at PC, multiple peaks appear within $d \approx 5-20$ Å, revealing that besides the docked glycan, other glycans can be partially docked in a relatively stable manner to the ConA surface.

II.I.II. Binding Energy Analysis—Docked MSGAs. The MSGA−ConA coupling strength can be described by its free energy of binding, ΔG, related to the dissociation constant, $K_d = \exp(\Delta G/k_B T)$. The experimental K_d values, shown in Figure 5C (bottom),[39] indicate that negatively charged MSGAs bind more strongly to ConA than positively charged ones, with the weakest binding observed for positively charged MSGAs.

The free energies of binding, ΔG, could be obtained by umbrella sampling methods, but it might be difficult to implement them precisely for these large and complex binders, with a gradual detachment of the docked glycans and the rest of MSGAs from ConA. Therefore, we examine the coupling in a two-step approach, where we first calculate the direct MSGAs−ConA binding energies when one glycan is docked in ConA (Figures 3 and 4), and then we separately calculate the residence times of MSGAs on ConA, once the glycan is undocked.

We first calculate the binding energies in the above simulations (Figures 3 and 4), where in each MSGA one glycan ligand is docked on ConA, while the rest of MSGA is freely attached to ConA surface around the docking site. Given a relatively weak nonspecific coupling of the rest of MSGA to ConA, its initial configuration does not play any role since the related phase space can be fast explored. In each simulated system, the frames within $t = 20-200$ ns are used to calculate the direct nonbonded energies (electrostatic, van der Waals contributions) by the NAMD Energy Plugin (Section III).

https://doi.org/10.1021/acs.jpcb.6c01091
J. Phys. Chem. B XXXX, XXX, XXX−XXX

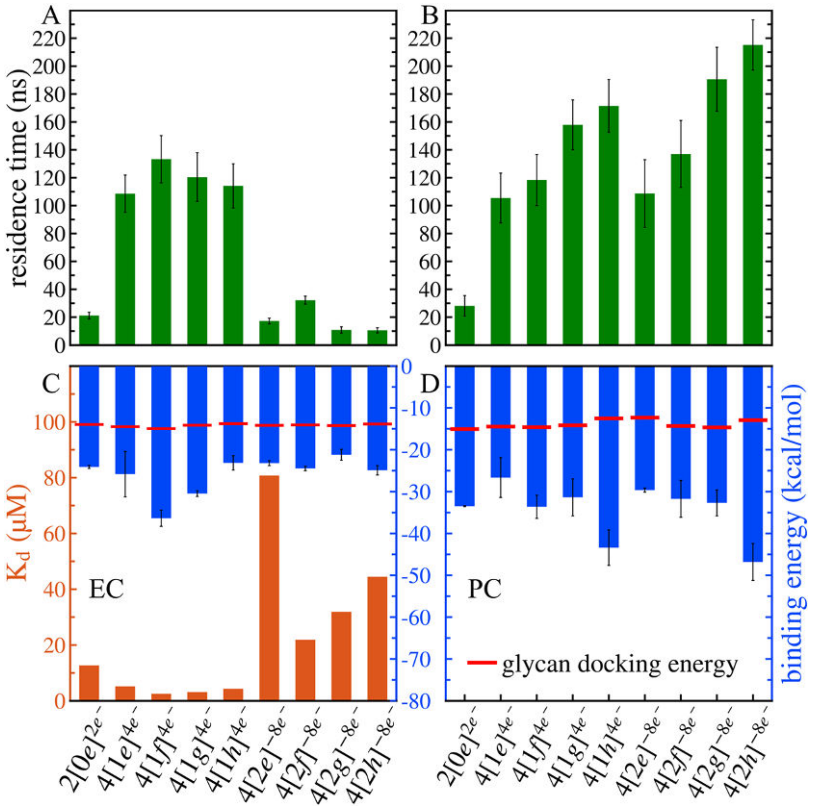


Figure 5. Residence times of MSGAs (undocked glycan) at ConA simulated at (A) EC and (B) PC. (C) (Top) Averaged nonbonded energies for each MSGA interacting with ConA, while one of its glycan is docked at EC from 20 to 200 ns. (D) The same was calculated at PC. Single glycan docking energy contributions are shown in horizontal lines. (C) (Bottom) Experimental K_d values obtained for MSGAs at EC.[38,39] Black error bars indicate histogram uncertainties.

Figure 5C (top) displays these energies, where the (red) horizontal lines show the glycan docking energies of $E_d \approx -14$ kcal/mol. Since E_d is the main contributor, these energies are relatively indifferent to MSGAs charging, except for several negative MSGAs. Figure 5D (top) reveals that slightly larger but still very similar energies are obtained for MSGAs at PC, where the repulsion or attraction of charged MSGAs to ConA is screened, allowing the formation of a better contact between them through the multivalent binding of many MSGAs-ligands (Figure 3). This may arise from slightly more stable multivalent contacts in PC, together with reduced PEG solubility relative to water (EC), which can promote solvent-mediated stabilization at the protein surface, and contribute to prolonged residence times.

The large similarity of direct binding energies (Figure 5) for these MSGAs might seem to contradict their very different experimental K_d values. These energies only represent the binding enthalpies obtained from microstates where one MSGA-glycan is docked in ConA, close to the docking site area (Figure 4). Once the docked glycan is released, MSGAs can stay or leave the site, depending on their coupling with ConA. These energies do not describe such decoupled microstates and do not cover other mostly entropic contributions to ΔG. Such contributions can be partly appreciated from MSGA-ConA residence times when all glycans are undocked.

II.I.III. Residence Time Analysis—Undocked MSGAs. Here, we calculate the MSGA-ConA residence times once the docked glycan is released from the docking site (starting position of the simulations). At EC, the residence time flow was terminated when MSGAs separated from ConA by more than the screening length, $\lambda_D \approx 3.04$ nm, while at PC, it was stopped when they separated by more than 3 Å. The averaging is done over three replicas.

Figure 5A shows that negatively charged MSGAs exhibit longer residence times on ConA, whereas positively charged MSGAs dissociate more rapidly. This trend reflects the underlying Coulombic attraction or repulsion between MSGAs and ConA, in agreement with the corresponding K_d values shown in Figure 5C. Figure 5B also shows these residence times at PC. They practically do not depend on the overall MSGA charges, but MSGAs with more valency and longer ligands have longer residence times. They also appear somewhat enhanced, even with respect to the attractive cases in EC.

II.II. Peptidoglycan Binder to ConA

While MSGAs provide a multivalent platform with good binding, their structural complexity and overall size might be less attractive for applications. The same might be true for other supramolecular constructs with glycan-functionalized peptide ligands.[40−43]

Here, we design and test a much simpler PG binder to ConA formed by a glycan EG-linked to a 10-residue-long peptide. The peptide is optimized by Rosetta[44−46] to achieve a highly specific binding to a ConA region near the glycan docking site. After identifying a sequence that interacted with this region in a stable manner, the peptide was connected through two EG monomers to the terminal glycan, as shown in Figure 6A. In this PG (glycan-EG-EG-CO-NH-SDNSSDRSCG-COOH), the N-terminus of the first residue (S1) was conjugated via a covalent amide bond to two EG monomers and the α-D-mannopyranos

https://doi.org/10.1021/acs.jpcb.6c01091
J. Phys. Chem. B XXXX, XXX, XXX−XXX

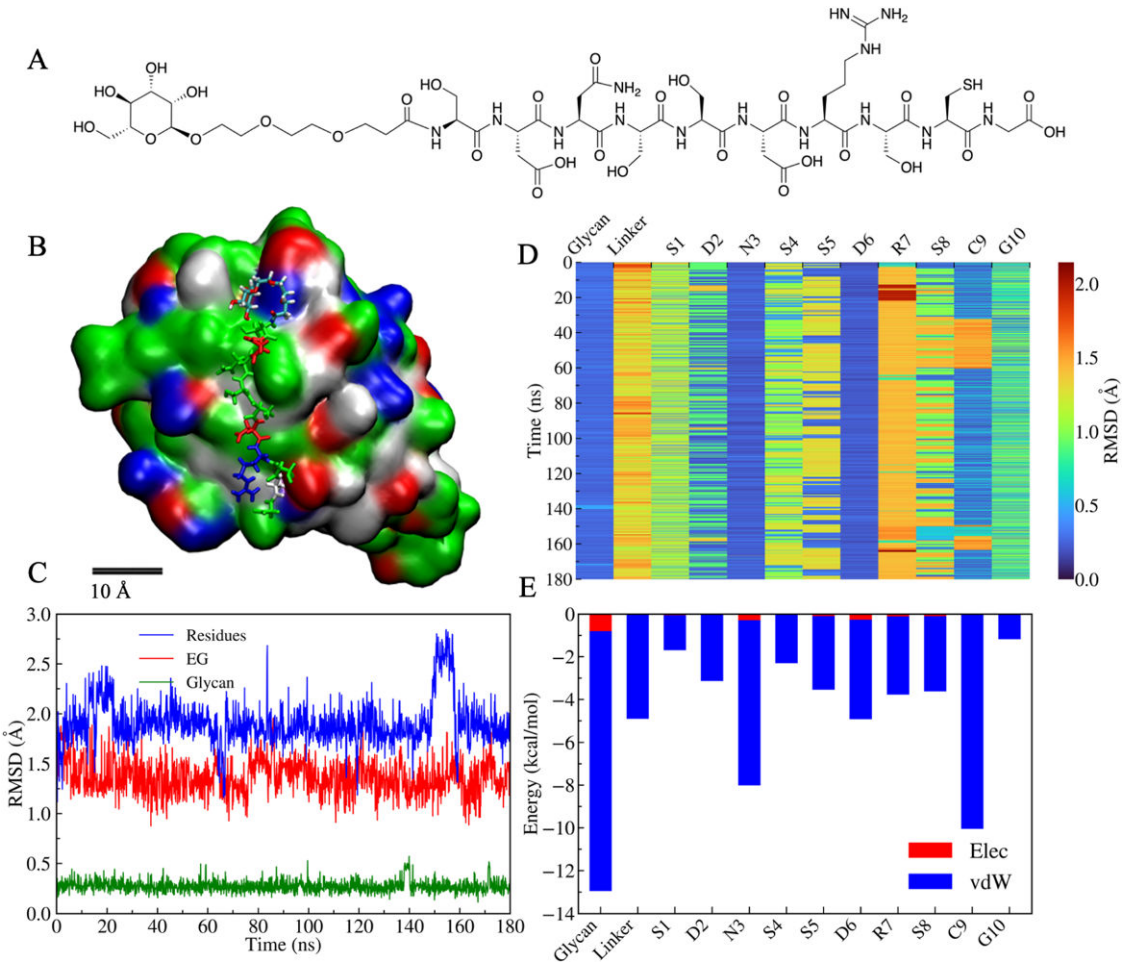


Figure 6. (A) Chemical structure of the glycan conjugated to EG units and the designed peptide. (B) Snapshot of this PG, docked on ConA, and freely simulated for 200 ns. Colors are based on residue types (red: acidic, blue: basic, green: polar, white: nonpolar). (C) Total RMSD of peptide, EG, and glycan. (D) RMSD for all PG residues, EG, and glycan. (E) Average energies for each residue, EG, and glycan.

glycan. The C-terminus is deprotonated under physiological conditions [COO^-].

This peptidoglycan was docked on ConA and simulated at PC for 200 ns (Section III), as shown in Figure 6B. The root-mean-square deviations (RMSD) of the PG components (glycan, linker, and peptide) indicate that the peptide interacts in a very stable manner with ConA (Figure 6C). The glycan is tightly docked, exhibiting the lowest RMSD, while the flexible linker shows a large RMSD, as expected. The whole peptide also has a relatively large RMSD. However, this is not true for many of the residues, separately presented in Figure 6D. In particular, the N3, D6, and C9 residues show a high stability.

These observations are supported by the direct binding energies of PG components to ConA, presented in Figure 6E. The data reveal a dominant role of van der Waals interactions in stabilizing the PG-ConA complex with a total binding energy of $E \approx -58.36 \pm 1$ kcal/mol (averaging over 20−200 ns) (Section III). This value is larger than the biggest binding energy of $E \approx -50.55$ kcal/mol acquired by $4[2(h)]^{-8\epsilon^-}$. In this strong PG-ConA binding, the glycan contributes by $E \approx -13$ kcal/mol, the peptide with a highly specific binding contributes by $E \approx -32.5$ kcal/mol, and the polar EG linker contributes by $E \approx -5$ kcal/mol. Further analysis indicates that the largest contributions come from N3 and C9, revealing that this binding is largely driven by a steric complementarity and favorable packing of small polar residues. Given the small size of PG, the interaction energy per unit of mass would be larger than in MSGAs. To relate further the results obtained by MSGAs and PG, we have separately simulated PG starting from its glycan-undocked configuration. The peptide part of PG remained localized at the specific ConA binding site for at least 1 μs, comparable to the longest MSGA residence times shown in Figure 5.

III. METHODS

The studied MSGAs were simulated at EC/PC with NAMD3.0.[47] ConA and ligands were described by the CHARMM36 force field.[48,49] At PC (pH = 7.4 and 150 mM NaCl), the ConA monomer (PDB ID: 1GKB)[50] carries a $7e^-$ net charge. At EC (pH = 4.8 and 10 mM NaCl), some residues in ConA (H24, H51, H121, H205, D10, D28, and E102) were protonated based on their pK_a values and their occurrence in ConA, using CHARMM-GUI,[51,52] making ConA overall neutral. The force-field parameters for the metallic core of the MSGAs were obtained in first-principles calculations at the MP2/def2-TZVP level using Gaussian.[53] Electrostatic potential (ESP)-derived partial charges, obtained at the same level of theory, were also used in the force field. During the simulations, each MSGA-Fe^{2+} ion and its six neighboring N atoms were arranged in an octahedral geometry, with all bond angles set to 90° and bond lengths fixed at 1.86 Å relative to one another using a harmonic potential with a spring force of k = 400 N/m. This angle fixation is based on the octahedral Fe^{2+} coordination, so the MSGA geometries should be reasonable.

https://doi.org/10.1021/acs.jpcb.6c01091
J. Phys. Chem. B XXXX, XXX, XXX−XXX

The systems were simulated in an NPT ensemble (p = 1 bar and T = 298 K) by the Langevin dynamics with a damping constant of γ_{Lang} = 4 ps^{-1}, preserving a realistic viscosity of water during the MSGA motion. The simulation time step was 2 fs. The van der Waals (L-J potential) and Coulombic interactions had cutoffs of 10 Å. The long-range Coulombic interactions were calculated by the PME method when periodic boundary conditions were applied.[54]

Initially, each MSGA was equilibrated in the proper solution. Then, it was placed on the top of ConA, where, in the docked simulations, one of the MSGA-ligand glycans were initially placed in the ConA receptor binding site (PDB ID: 4PF5)[55] Although one glycan was initially placed in the binding site to define a docked starting state, no restraints were applied, so the binder remained free to dissociate and sample alternative binding modes, allowing unbiased sampling of interaction dynamics. In the undocked simulations (residence time studies), one glycan was positioned near the binding site of ConA to examine how MSGA explores the protein surface once the glycan exits the binding site. The equilibration began with a 2 ns long initial phase (ion redistribution) in which MSGA and ConA were placed in separate harmonic potentials with a force constant of k = 1 kcal/mol $Å^2$, while the metal ions in ConA were placed in a harmonic potential with k = 10 kcal/mol $Å^2$. Subsequently, the constraints on the system were released, except for the ConA backbone and its metal ions. Then, the systems were simulated for 200 ns (docked cases) or until MSGA leaves ConA (undocked cases). Three independent replicas of each simulation were performed.

Initially, the PG peptide was designed using a simple method.[56] Since the initial 10-residue peptide, KPRLDFGRCF, did not exhibit strong binding around the glycan binding site, it was refined using Rosetta. The initial structure was first subjected to constrained relaxation using the Rosetta relax protocol[57] to remove potential steric clashes and optimize local backbone and side-chain conformations, while preserving the overall binding geometry. Then, further sequence optimization was performed using a fixed-backbone design protocol (fixbb),[58] with enhanced rotamer sampling (-ex1, -ex2) and input side-chain preservation. To further refine peptide−protein interactions and improve interface packing, high-resolution flexible peptide docking was carried out using the FlexPepDock refinement protocol[59] with expanded side-chain sampling (-ex1, -ex2aro), generating 50 refined models per design. All models were ranked based on Rosetta energy scores, and top-scoring conformations were selected for subsequent analysis. Output structures and score files were saved for structural and energetic evaluation. The final peptide sequence was selected from Rosetta design as the lowest-scoring candidate, corresponding to the most favorable predicted binding and structural stability among the sampled sequences.

The PG energy was calculated in the same way as that for MSGAs. The RMSD was calculated using the PG atoms belonging to the specific segment of interest (backbone for the peptide and heavy atoms for the linker and glycan). In all cases, the initial docked structure of the corresponding segment was used as the reference structure.

IV. CONCLUSION

We have simulated glycoconjugate lectin binders of different topologies, charges, and linkers. First, we simulated metal-losupramolecular-glycans binding to ConA. The simulations have revealed that the strength of multivalent binding increases with the length of PEG ligands used in these MSGAs, which can reach more distant regions of ConA. However, in physiological solutions, the overall charge of each MSGA practically does not play any role. Next, we designed and simulated significantly smaller peptidoglycan binders to ConA, and found that their highly specific binding strengths are comparable to MSGAs. These examples illustrate that larger and less specific multivalent binders can have similar avidities to target receptors as smaller, more-specific binders. These results demonstrate that highly specific small-peptide-based binders can match much less specific multivalent binders. Therefore, PGs can serve as effective and tunable binders of lectins and other receptors. These observations could be implemented in the design of therapeutics[60] and other biomedical applications.[61,62]

AUTHOR INFORMATION

Corresponding Author

Petr Král − *Department of Chemistry, University of Illinois Chicago, Chicago, Illinois 60607, United States; Departments of Physics, Pharmaceutical Sciences, and Chemical Engineering, University of Illinois Chicago, Chicago, Illinois 60607, United States;* orcid.org/0000-0003-2992-9027; Email: pkral@uic.edu

Author

Roya Jafari − *Department of Chemistry, University of Illinois Chicago, Chicago, Illinois 60607, United States*

Complete contact information is available at: https://pubs.acs.org/10.1021/acs.jpcb.6c01091

Notes

The authors declare no competing financial interest.

ACKNOWLEDGMENTS

P.K. acknowledges support from NSF DMR 2212123. We would like to thank Julia M. Stauber for helpful discussions.

REFERENCES

(1) Raposo, C. D.; Canelas, A. B.; Barros, M. T. Human Lectins, Their Carbohydrate Affinities and Where to Find Them. *Biomolecules* **2021**, *11*, 188.

(2) Air, G. M. The Role of Carbohydrates in Viral Infections. In *Carbohydrate Recognition: Biological Problems, Methods, and Applications*; Wang, B., Ed.; John Wiley & Sons: Hoboken, NJ, 2011; pp 65−91.

(3) Flannery, A.; Gerlach, J. Q.; Joshi, L.; Kilcoyne, M. Assessing bacterial interactions using carbohydrate-based microarrays. *Microarrays* **2015**, *4*, 690−713.

(4) Wittmann, V.; Pieters, R. J. Bridging lectin binding sites by multivalent carbohydrates. *Chem. Soc. Rev.* **2013**, *42*, 4492−4503.

(5) Johannssen, T.; Lepenies, B. Glycan-based cell targeting to modulate immune responses. *Trends Biotechnol.* **2017**, *35*, 334−346.

(6) Pinho, S. S.; Alves, I.; Gaifem, J.; Rabinovich, G. A. Immune regulatory networks coordinated by glycans and glycan-binding proteins in autoimmunity and infection. *Cell. Mol. Immunol.* **2023**, *20*, 1101−1113.

(7) Rabinovich, G. A.; Croci, D. O. Regulatory circuits mediated by lectin−glycan interactions in autoimmunity and cancer. *Immunity* **2012**, *36*, 322−335.

(8) Cho, S. H.; Park, J. Y.; Kim, C. H. Systemic lectin−glycan interaction of pathogenic enteric bacteria in the gastrointestinal tract. *Int. J. Mol. Sci.* **2022**, *23*, 1451.

(9) Han, Y.; Král, P. Computational design of ACE2-based peptide inhibitors of SARS-CoV-2. *ACS Nano* **2020**, *14*, 5143−5147.

(10) Leusmann, S.; Ménová, P.; Shanin, E.; Titz, A.; Rademacher, C. Glycomimetics for the inhibition and modulation of lectins. *Chem. Soc. Rev.* **2023**, *52*, 3663−3740.

(11) Coppola, F.; Jafari, R.; McReynolds, K. D.; Král, P. Sulfoglycodendron antivirals with scalable architectures and activities. *J. Chem. Inf. Model.* **2024**, *64*, 7141−7151.

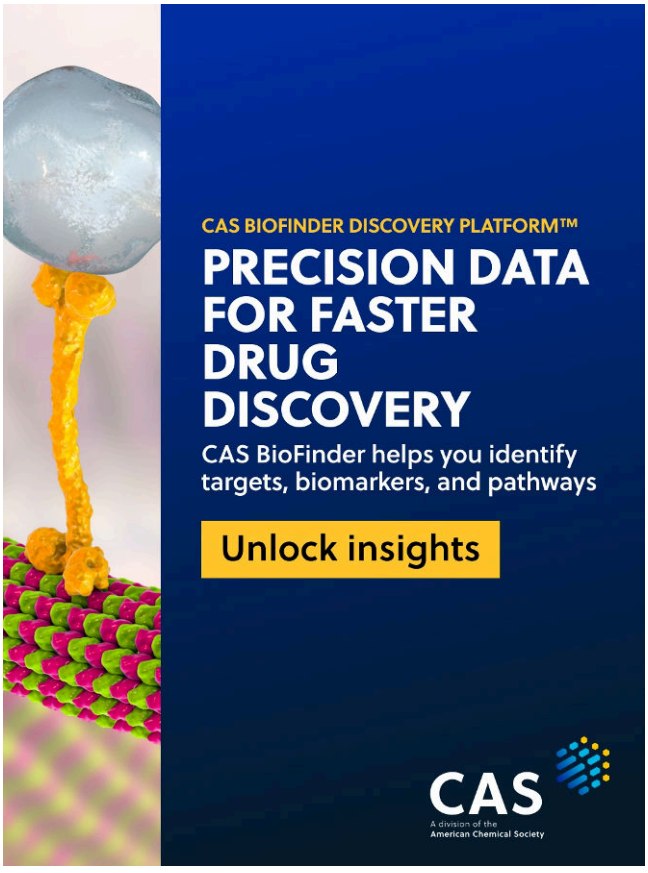
(12) Kiessling, L. L.; Young, T.; Gruber, T. D.; Mortell, K. H. Multivalency in protein-carbohydrate recognition. *Glycoscience* **2008**, 2483−2523.

(13) Sen, S.; Han, Y.; Rehak, P.; Vukovic, L.; Král, P. Computational Studies of Micellar and Nanoparticle Nanomedicines. *Chem. Soc. Rev.* **2018**, *47*, 3849−3860.

(14) Loka, R. S.; McConnell, M. S.; Nguyen, H. M. Studies of highly-ordered heterodiantennary mannose/glucose-functionalized polymers and concanavalin A protein interactions using isothermal titration calorimetry. *Biomacromolecules* **2015**, *16*, 4013−4021.
(15) Martínez-Bailén, M.; Rojo, J.; Ramos-Soriano, J. Multivalent glycosystems for human lectins. *Chem. Soc. Rev.* **2023**, *52*, 536−572.
(16) Spinelli, N.; Defrancq, E.; Morvan, F. Glycoclusters on oligonucleotide and PNA scaffolds: synthesis and applications. *Chem. Soc. Rev.* **2013**, *42*, 4557−4573.
(17) Richards, S.-J.; Gibson, M. I. Toward glycomaterials with selectivity as well as affinity. *JACS Au* **2021**, *1*, 2089−2099.
(18) Percec, V.; Leowanawat, P.; Sun, H.-J.; Kulikov, O.; Nusbaum, C. D.; Tran, T. M.; Bertin, A.; Wilson, D. A.; Peterca, M.; Zhang, S.; Heiney, P. A.; et al. Modular synthesis of amphiphilic Janus glycodendrimers and their self-assembly into glycodendrimersomes and other complex architectures with bioactivity to biomedically relevant lectins. *J. Am. Chem. Soc.* **2013**, *135*, 9055−9077.
(19) Zhang, S.; Moussodia, R.-O.; Sun, H.-J.; Leowanawat, P.; Muncan, A.; Nusbaum, C. D.; Chelling, K. M.; Heiney, P. A.; Klein, M. L.; Percec, V.; et al. Mimicking biological membranes with programmable glycan ligands self-assembled from amphiphilic Janus glycodendrimers. *Angew. Chem.* **2014**, *126*, 11079−11083.
(20) Marradi, M.; Martin-Lomas, M.; Penadés, S. Glyconanoparticles: Polyvalent tools to study carbohydrate-based interactions. *Adv. Carbohydr. Chem. Biochem.* **2010**, *64*, 211−290.
(21) Yilmaz, G.; Becer, C. R. Glyconanoparticles and their interactions with lectins. *Polym. Chem.* **2015**, *6*, 5503−5514.
(22) Müller, C.; Despras, G.; Lindhorst, T. K. Organizing multivalency in carbohydrate recognition. *Chem. Soc. Rev.* **2016**, *45*, 3275−3302.
(23) Brewer, C. F. Binding and cross-linking properties of galectins. *Biochim. Biophys. Acta* **2002**, *1572*, 255−262.
(24) Roy, R.; Murphy, P. V.; Gabius, H.-J. Multivalent carbohydrate-lectin interactions: How synthetic chemistry enables insights into nanometric recognition. *Molecules* **2016**, *21*, 629.
(25) Mende, M.; Bordoni, V.; Tsouka, A.; Loeffler, F. F.; Delbianco, M.; Seeberger, P. H. Multivalent glycan arrays. *Faraday Discuss.* **2019**, *219*, 9−32.
(26) Zhou, F.; Li, S.; Cook, T. R.; He, Z.; Stang, P. J. Saccharide-functionalized organoplatinum (II) metallacycles. *Organometallics* **2014**, *33*, 7019−7022.
(27) Qian, E. A.; Wixtrom, A. I.; Axtell, J. C.; Saebi, A.; Jung, D.; Rehak, P.; Han, Y.; et al. Atomically precise organomimetic cluster nanomolecules assembled via perfluoroaryl-thiol SNAr chemistry. *Nat. Chem.* **2017**, *9*, 333−340.
(28) Hwang, S.-H.; Shreiner, C. D.; Moorefield, C. N.; Newkome, G. R. Recent progress and applications for metallosupramoleculars. *New J. Chem.* **2007**, *31*, 1192−1217.
(29) Sepehrpour, H.; Fu, W.; Sun, Y.; Stang, P. J. Biomedically relevant self-assembled metallacycles and metallacages. *J. Am. Chem. Soc.* **2019**, *141*, 14005−14020.
(30) Mohy El Dine, T.; Jimmidi, R.; Diaconu, A.; Fransolet, M.; Michiels, C.; De Winter, J.; Gillon, E.; Imberty, A.; Coenye, T.; Vincent, S. P. Pillar[5]arene-based polycationic glyco[2]rotaxanes designed as Pseudomonas aeruginosa antibiofilm agents. *J. Med. Chem.* **2021**, *64*, 14728−14744.
(31) Pritchard, C.; Ligorio, M.; Jackson, G. D.; Gibson, M. I.; Ward, M. D. Programmable Monodisperse Glyco-Multivalency Using Self-Assembled Coordination Cages as Scaffolds. *ACS Appl. Mater. Interfaces* **2023**, *15*, 36052−36060.
(32) Tang, Y.-H.; Huang, A. Y.-T.; Chen, P.-Y.; Chen, H.-T.; Kao, C.-L. Metallosupramoleculars and dendrimer nanocomposites. *Curr. Pharm. Des.* **2011**, *17*, 2308−2330.
(33) Govender, P.; Therrien, B.; Smith, G. S. Bio-metallosupramoleculars—emerging strategies in metal-based drug design. *Eur. J. Inorg. Chem.* **2012**, *2012*, 2853−2862.
(34) Burke, B. P.; Grantham, W.; Burke, M. J.; Nichol, G. S.; Roberts, D.; Renard, I.; Hargreaves, R.; Cawthorne, C.; Archibald, S. J.; Lusby, P. J. Visualizing kinetically robust CoIII4L6 assemblies in vivo: SPECT imaging of the encapsulated [99mTc] TcO4-anion. *J. Am. Chem. Soc.* **2018**, *140*, 16877−16881.
(35) Khan, S. A.; Adak, A.; Murthy, R. V.; Kikkeri, R. Recent advances in the metallo-glycodendrimers and its potential applications. *Inorg. Chim. Acta* **2014**, *409*, 26−33.
(36) Moffett, S.; Shiao, T. C.; Mousavifar, L.; Mignani, S.; Roy, R. Aberrant glycosylation patterns on cancer cells: Therapeutic opportunities for glycodendrimers/metallosupramoleculars oncology. *Wiley Interdiscip. Rev. Nanomed. Nanobiotechnol.* **2021**, *13*, e1659.
(37) Benkovska, D.; Flodrova, D.; Bobalova, J. Application of monolithic affinity HPLC column for rapid determination of malt glycoproteins. *J. Liq. Chromatogr. Relat. Technol.* **2013**, *36*, 561−572.
(38) Schwab, J. H.; Bailey, J. B.; Gembicky, M.; Stauber, J. M. Programmable synthesis of well-defined, glycosylated iron(II) supramolecular assemblies with multivalent protein-binding capabilities. *Chem. Sci.* **2023**, *14*, 1018−1026.
(39) Stauber, J. M. Tailoring metallosuparamolecular glycoassemblies for enhancing lectin recognition. *Angew. Chem., Int. Ed.* **2024**, *63*, No. e202408751.
(40) Tsouka, A.; Hoetzel, K.; Mende, M.; Heidepriem, J.; Paris, G.; Eickelmann, S.; Seeberger, P. H.; Lepenies, B.; Loeffler, F. F. Probing multivalent carbohydrate−protein interactions with on-chip synthesized glycopeptides using different functionalized surfaces. *Front. Chem.* **2021**, *9*, 766932.
(41) Pifferi, C.; Thomas, B.; Goyard, D.; Berthet, N.; Renaudet, O. Heterovalent glycodendrimers as epitope carriers for antitumor synthetic vaccines. *Chem. − Eur. J.* **2017**, *23*, 16283−16296.
(42) Goyard, D.; Martin-Serrano Ortiz, A.; Boturyn, D.; Renaudet, O. Multivalent glycocyclopeptides: conjugation methods and biological applications. *Chem. Soc. Rev.* **2022**, *51*, 8756−8783.
(43) Lusvarghi, S.; Ghirlando, R.; Wong, C.-H.; Bewley, C. A. Glycopeptide mimetics recapitulate high-mannose-type oligosaccharide binding and function. *Angew. Chem., Int. Ed.* **2015**, *54*, 5603−5608.
(44) Leaver-Fay, A.; Tyka, M.; Lewis, S. M.; Lange, O. F.; Thompson, J.; Jacak, R.; Kaufman, K. W.; et al. ROSETTA3: an object-oriented software suite for the simulation and design of macromolecules. *Methods Enzymol.* **2011**, *487*, 545−574.
(45) Fleishman, S. J.; Leaver-Fay, A.; Corn, J. E.; Strauch, E.-M.; Khare, S. D.; Koga, N.; Ashworth, J.; et al. RosettaScripts: a scripting language interface to the Rosetta macromolecular modeling suite. *PLoS One* **2011**, *6*, e20161.
(46) Leman, J. K.; Weitzner, B. D.; Lewis, S. M.; Adolf-Bryfogle, J.; Alam, N.; Alford, R. F.; Aprahamian, M.; et al. Macromolecular modeling and design in Rosetta: recent methods and frameworks. *Nat. Methods* **2020**, *17*, 665−680.
(47) Phillips, J. C.; Hardy, D. J.; Maia, J. D. C.; Stone, J. E.; Ribeiro, J. V.; Bernardi, R. C.; Buch, R.; Fiorin, G.; Hénin, J.; Jiang, W.; et al. Scalable molecular dynamics on CPU and GPU architectures with NAMD. *J. Chem. Phys.* **2020**, *153*, 044130.
(48) Brooks, B. R.; Bruccoleri, R. E.; Olafson, B. D.; States, D. J.; Swaminathan, S.; Karplus, M. CHARMM: a program for macromolecular energy, minimization, and dynamics calculations. *J. Comput. Chem.* **1983**, *4*, 187−217.
(49) Brooks, B. R.; Brooks, C. L., III; Mackerell, A. D., Jr.; Nilsson, L.; Petrella, R. J.; Roux, B.; Won, Y.; Archontis, G.; Bartels, C.; Boresch, S.; et al. CHARMM: the biomolecular simulation program. *J. Comput. Chem.* **2009**, *30*, 1545−1614.
(50) Kantardjieff, K. A.; Hoechtl, P.; Segelke, B. W.; Tao, F.-M.; Rupp, B. Concanavalin A in a dimeric crystal form: revisiting structural accuracy and molecular flexibility. *Acta Crystallogr., Sect. D* **2002**, *58*, 735−743.
(51) Jo, S.; Kim, T.; Iyer, V. G.; Im, W. CHARMM-GUI: A Web-Based Graphical User Interface for CHARMM. *J. Comput. Chem.* **2008**, *29*, 1859−1865.
(52) Wu, E. L.; Cheng, X.; Jo, S.; Rui, H.; Song, K. C.; Dávila-Contreras, E. M.; Qi, Y.; Lee, J.; Monje-Galvan, V.; Venable, R. M.et al. *CHARMM-GUI Membrane Builder Toward Realistic Biological Membrane Simulations*; Wiley Online Library, 2014.

https://doi.org/10.1021/acs.jpcb.6c01091
J. Phys. Chem. B XXXX, XXX, XXX−XXX

(53) Frisch, M. J.et al. *Gaussian 09*, Revision D.01; Gaussian, Inc.: Wallingford, CT, 2009.
(54) Cheatham, T. E. I., III; Miller, J. L.; Fox, T.; Darden, T. A.; Kollman, P. A. Molecular dynamics simulations on solvated biomolecular systems: The particle mesh Ewald method leads to stable trajectories of DNA, RNA, and proteins. *J. Am. Chem. Soc.* **1995**, *117*, 4193−4194.
(55) François-Heude, M.; Méndez-Ardoy, A.; Cendret, V.; Lafite, P.; Daniellou, R.; Ortiz Mellet, C.; Garcia Fernandez, J. M.; Moreau, V.; Djedaïni-Pilard, F. Synthesis of High-Mannose Oligosaccharide Analogues through Click Chemistry: True Functional Mimics of Their Natural Counterparts Against Lectins? *Chem. − Eur. J.* **2015**, *21*, 1978−1991.
(56) Coppola, F.; Král, P. On-the-Fly Sequential Design of Simple Peptides. *J. Chem. Inf. Model.* **2025**, *65*, 9738−9746, DOI: 10.1021/acs.jcim.5c01340.
(57) Khatib, F.; Cooper, S.; Tyka, M. D.; Xu, K.; Makedon, I.; Popović, Z.; Baker, D. Foldit Players. Algorithm discovery by protein folding game players. *Proc. Natl. Acad. Sci. U.S.A.* **2011**, *108*, 18949−18953.
(58) Lyskov, S.; Chou, F.-C.; Conchuir, S. O.; Der, B. S.; Drew, K.; Kuroda, D.; Xu, J.; et al. Serverification of molecular modeling applications: the Rosetta Online Server that Includes Everyone (ROSIE). *PLoS One* **2013**, *8*, e63906.
(59) London, N.; Raveh, B.; Cohen, E.; Fathi, G.; Schueler-Furman, O. Rosetta FlexPepDock web server—high-resolution modeling of peptide−protein interactions. *Nucleic Acids Res.* **2011**, *39*, W249−W253.
(60) Woods, B.; Silva, R. D. M.; Schmidt, C.; Wragg, D.; Cavaco, M.; Neves, V.; Ferreira, V. F. C.; Gano, L.; Morais, T. S.; Mendes, F.; et al. Bioconjugate supramolecular Pd^{2+} metallcages penetrate the blood brain barrier in vitro and in vivo. *Bioconjugate Chem.* **2021**, *32*, 1399−1408.
(61) Casini, A.; Woods, B.; Wenzel, M. The promise of self-assembled 3D supramolecular coordination complexes for biomedical applications. *Inorg. Chem.* **2017**, *56*, 14715−14729.
(62) Wang, Y.-P.; Zhang, Y.; Duan, X.-H.; Mao, J.-J.; Pan, M.; Shen, J.; Su, C.-Y. Recent progress in metal-organic cages for biomedical application: Highlighted research during 2018−2023. *Coord. Chem. Rev.* **2024**, *501*, 215570.



https://doi.org/10.1021/acs.jpcb.6c01091
J. Phys. Chem. B XXXX, XXX, XXX−XXX